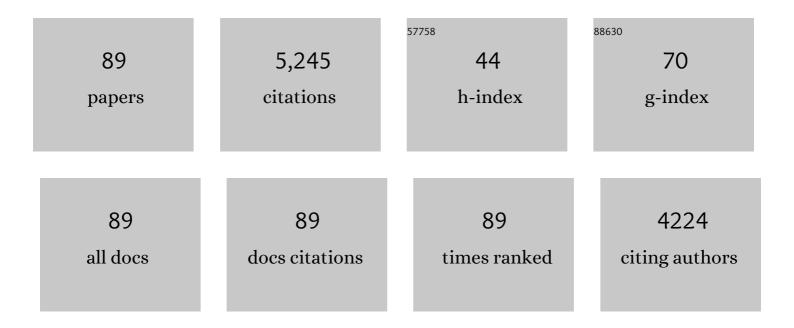
Kheibar Dashtian

List of Publications by Year in descending order

Source: https://exaly.com/author-pdf/6229634/publications.pdf Version: 2024-02-01



#	Article	IF	CITATIONS
1	Ultrasonically assisted hydrothermal synthesis of activated carbon–HKUST-1-MOF hybrid for efficient simultaneous ultrasound-assisted removal of ternary organic dyes and antibacterial investigation: Taguchi optimization. Ultrasonics Sonochemistry, 2016, 31, 383-393.	8.2	267
2	Sonochemical-assisted synthesis of CuO/Cu2O/Cu nanoparticles as efficient photocatalyst for simultaneous degradation of pollutant dyes in rotating packed bed reactor: LED illumination and central composite design optimization. Ultrasonics Sonochemistry, 2018, 40, 601-610.	8.2	202
3	Highly efficient simultaneous ultrasonic assisted adsorption of brilliant green and eosin B onto ZnS nanoparticles loaded activated carbon: Artificial neural network modeling and central composite design optimization. Spectrochimica Acta - Part A: Molecular and Biomolecular Spectroscopy, 2016, 153, 257-267.	3.9	160
4	Ultrasonic enhancement of the simultaneous removal of quaternary toxic organic dyes by CuO nanoparticles loaded on activated carbon: Central composite design, kinetic and isotherm study. Ultrasonics Sonochemistry, 2016, 31, 546-557.	8.2	149
5	Preparation and Characterization of Mn _{0.4} Zn _{0.6} Fe ₂ O ₄ Nanoparticles Supported on Dead Cells of <i>Yarrowia lipolytica</i> as a Novel and Efficient Adsorbent/Biosorbent Composite for the Removal of Azo Food Dyes: Central Composite Design Optimization Study. ACS Sustainable Chemistry	6.7	142
6	and Engineering, 2018, b. 4644-6563 Photocatalytic degradation of binary mixture of toxic dyes by HKUST-1 MOF and HKUST-1-SBA-15 in a rotating packed bed reactor under blue LED illumination: central composite design optimization. RSC Advances, 2016, 6, 17204-17214.	3.6	140
7	Sonophotocatalytic degradation of trypan blue and vesuvine dyes in the presence of blue light active photocatalyst of Ag3PO4/Bi2S3-HKUST-1-MOF: Central composite optimization and synergistic effect study. Ultrasonics Sonochemistry, 2016, 32, 387-397.	8.2	136
8	Rapid ultrasound-assisted magnetic microextraction of gallic acid from urine, plasma and water samples by HKUST-1-MOF-Fe3O4-GA-MIP-NPs: UV–vis detection and optimization study. Ultrasonics Sonochemistry, 2017, 34, 561-570.	8.2	132
9	Enhanced simultaneous removal of malachite green and safranin O by ZnO nanorod-loaded activated carbon: modeling, optimization and adsorption isotherms. New Journal of Chemistry, 2015, 39, 7998-8005.	2.8	130
10	Achieving enhanced blue-light-driven photocatalysis using nanosword-like VO2/CuWO4 type II n–n heterojunction. Chemical Engineering Journal, 2018, 339, 189-203.	12.7	123
11	Central composite design and genetic algorithm applied for the optimization of ultrasonic-assisted removal of malachite green by ZnO Nanorod-loaded activated carbon. Spectrochimica Acta - Part A: Molecular and Biomolecular Spectroscopy, 2016, 167, 157-164.	3.9	114
12	Fe3O4-FeMoS4: Promise magnetite LDH-based adsorbent for simultaneous removal of Pb (II), Cd (II), and Cu (II) heavy metal ions. Journal of Hazardous Materials, 2021, 410, 124560.	12.4	113
13	Sonochemical assisted hydrothermal synthesis of ZnO: Cr nanoparticles loaded activated carbon for simultaneous ultrasound-assisted adsorption of ternary toxic organic dye: Derivative spectrophotometric, optimization, kinetic and isotherm study. Ultrasonics Sonochemistry, 2016, 32, 119-131	8.2	110
14	Ultrasound-assisted removal of Al ³⁺ ions and Alizarin red S by activated carbon engrafted with Ag nanoparticles: central composite design and genetic algorithm optimization. RSC Advances, 2015, 5, 59522-59532.	3.6	109
15	Ultrasound assisted combined molecularly imprinted polymer for selective extraction of nicotinamide in human urine and milk samples: Spectrophotometric determination and optimization study. Ultrasonics Sonochemistry, 2017, 34, 640-650.	8.2	106
16	BiPO ₄ /Bi ₂ S ₃ -HKUST-1-MOF as a novel blue light-driven photocatalyst for simultaneous degradation of toluidine blue and auramine-O dyes in a new rotating packed bed reactor: optimization and comparison to a conventional reactor. RSC Advances, 2016, 6, 63667-63680.	3.6	103
17	Ultrasonic-assisted magnetic solid phase extraction of morphine in urine samples by new imprinted polymer-supported on MWCNT-Fe3O4-NPs: Central composite design optimization. Ultrasonics Sonochemistry, 2016, 33, 240-248.	8.2	100
18	Synthesis and characterization of functionalized mesoprous SBA-15 decorated with Fe3O4 nanoparticles for removal of Ce(III) ions from aqueous solution: ICP–OES detection and central composite design optimization. Journal of Colloid and Interface Science, 2017, 494, 114-123.	9.4	97

KHEIBAR DASHTIAN

#	Article	IF	CITATIONS
19	New MOF/COF Hybrid as a Robust Adsorbent for Simultaneous Removal of Auramine O and Rhodamine B Dyes. ACS Omega, 2020, 5, 9420-9428.	3.5	95
20	Preparation and characterization of MWCNTs functionalized by N-(3-nitrobenzylidene)-Nâ€2-trimethoxysilylpropyl-ethane-1,2-diamine for the removal of aluminum(<scp>iii</scp>) ions via complexation with eriochrome cyanine R: spectrophotometric detection and optimization. RSC Advances, 2015, 5, 61060-61069.	3.6	94
21	Ag 3 PO 4 /AgBr/Ag-HKUST-1-MOF composites as novel blue LED light active photocatalyst for enhanced degradation of ternary mixture of dyes in a rotating packed bed reactor. Chemical Engineering and Processing: Process Intensification, 2017, 114, 24-38.	3.6	94
22	New ion-imprinted polymer-functionalized mesoporous SBA-15 for selective separation and preconcentration of Cr(<scp>iii</scp>) ions: modeling and optimization. RSC Advances, 2015, 5, 105789-105799.	3.6	90
23	Rapid and high-capacity ultrasonic assisted adsorption of ternary toxic anionic dyes onto MOF-5-activated carbon: Artificial neural networks, partial least squares, desirability function and isotherm and kinetic study. Ultrasonics Sonochemistry, 2017, 37, 71-82.	8.2	85
24	Simultaneous removal of methylene blue and Pb ²⁺ ions using ruthenium nanoparticle-loaded activated carbon: response surface methodology. RSC Advances, 2015, 5, 83427-83435.	3.6	83
25	Photo-Sensitive Pb5S2I6 crystal incorporated polydopamine biointerface coated on nanoporous TiO2 as an efficient signal-on photoelectrochemical bioassay for ultrasensitive detection of Cr(VI) ions. Biosensors and Bioelectronics, 2019, 132, 105-114.	10.1	76
26	L-phenylalanine-imprinted polydopamine-coated CdS/CdSe n-n type II heterojunction as an ultrasensitive photoelectrochemical biosensor for the PKU monitoring. Biosensors and Bioelectronics, 2020, 165, 112346.	10.1	76
27	UiO-66(Ti)-Fe3O4-WO3 photocatalyst for efficient ammonia degradation from wastewater into continuous flow-loop thin film slurry flat-plate photoreactor. Journal of Hazardous Materials, 2020, 393, 122360.	12.4	74
28	Novel nanorose-like Ce(<scp>iii</scp>)-doped and undoped Cu(<scp>ii</scp>)–biphenyl-4,4-dicarboxylic acid (Cu(<scp>ii</scp>)–BPDCA) MOSs as visible light photocatalysts: synthesis, characterization, photodegradation of toxic dyes and optimization. Physical Chemistry Chemical Physics, 2016, 18, 11278-11287.	2.8	73
29	A review on metal-organic frameworks photoelectrochemistry: A headlight for future applications. Coordination Chemistry Reviews, 2021, 445, 214097.	18.8	70
30	Preparation and characterization of an ACâ€"Fe ₃ O ₄ â€"Au hybrid for the simultaneous removal of Cd ²⁺ , Pb ²⁺ , Cr ³⁺ and Ni ²⁺ ions from aqueous solution via complexation with 2-((2,4-dichloro-benzylidene)-amino)-benzenethiol: Taguchi optimization. RSC Advances, 2016, 6,	3.6	67
31	19780-19791. HKUST-1-MOF–BiVO ₄ hybrid as a new sonophotocatalyst for simultaneous degradation of disulfine blue and rose bengal dyes: optimization and statistical modelling. RSC Advances, 2016, 6, 61516-61527.	3.6	66
32	Novel visible light-driven Cu-based MOFs/Ag ₂ O composite photocatalysts with enhanced photocatalytic activity toward the degradation of orange G: their photocatalytic mechanism and optimization study. New Journal of Chemistry, 2018, 42, 9720-9734.	2.8	65
33	Adsorption of semisoft pollutants onto Bi 2 S 3 /Ag 2 S-AC under the influence of ultrasonic waves as external filed. Journal of Industrial and Engineering Chemistry, 2018, 60, 390-400.	5.8	62
34	Back propagation artificial neural network and central composite design modeling of operational parameter impact for sunset yellow and azur (II) adsorption onto MWCNT and MWCNT-Pd-NPs: Isotherm and kinetic study. Chemometrics and Intelligent Laboratory Systems, 2016, 159, 127-137.	3.5	60
35	Bi ₂ WO ₆ /Ag ₃ PO ₄ –Ag Z-scheme heterojunction as a new plasmonic visible-light-driven photocatalyst: performance evaluation and mechanism study. New Journal of Chemistry, 2019, 43, 1275-1284.	2.8	58
36	Ti-Based Solid-State Imprinted-Cu2O/CuInSe2 Heterojunction Photoelectrochemical platform for Highly Selective Dopamine Monitoring. Sensors and Actuators B: Chemical, 2021, 326, 128824.	7.8	58

#	Article	IF	CITATIONS
37	Simultaneous removing of Pb2+ ions and alizarin red S dye after their complexation by ultrasonic waves coupled adsorption process: Spectrophotometry detection and optimization study. Ultrasonics Sonochemistry, 2017, 35, 51-60.	8.2	57
38	Chitosan extraction from lobster shells and its grafted with functionalized MWCNT for simultaneous removal of Pb 2+ ions and eriochrome cyanine R dye after their complexation. International Journal of Biological Macromolecules, 2017, 102, 181-191.	7.5	54
39	Ce/Eu redox couple functionalized HKUST-1 MOF insight to sono-photodegradation of malathion. Journal of Hazardous Materials, 2021, 409, 124478.	12.4	54
40	Simultaneous removal of Cd(II), Ni(II), Pb(II) and Cu(II) ions via their complexation with HBANSA based on a combined ultrasound-assisted and cloud point adsorption method using CSG-BiPO 4 /FePO 4 as novel adsorbent: FAAS detection and optimization process. Journal of Colloid and Interface Science, 2017, 500, 241-252.	9.4	53
41	Design of a new technique based on combination of ultrasound waves via magnetite solid phase and cloud point microextraction for determination of Cr(III) ions. Ultrasonics Sonochemistry, 2017, 39, 798-809.	8.2	52
42	Fe ₃ O ₄ -Based Melamine-Rich Covalent Organic Polymer for Simultaneous Removal of Auramine O and Rhodamine B. Journal of Chemical & Engineering Data, 2020, 65, 696-705.	1.9	52
43	CO2 capture by amine-based aqueous solution containing atorvastatin functionalized mesocellular silica foam in a counter-current rotating packed bed: Central composite design modeling. Chemical Engineering Research and Design, 2018, 129, 64-74.	5.6	50
44	One step integration of plasmonic Ag2CrO4/Ag/AgCl into HKUST-1-MOF as novel visible-light driven photocatalyst for highly efficient degradation of mixture dyes pollutants: Its photocatalytic mechanism and modeling. Polyhedron, 2019, 166, 217-225.	2.2	47
45	ZnO nanoparticles loaded different mesh size of porous activated carbon prepared from Pinus eldarica and its effects on simultaneous removal of dyes: Multivariate optimization. Chemical Engineering Research and Design, 2017, 125, 408-421.	5.6	46
46	MOF-5(Zn)-Fe 2 O 4 nanocomposite based magnetic solid-phase microextraction followed by HPLC-UV for efficient enrichment of colchicine in root of colchicium extracts and plasma samples. Journal of Chromatography B: Analytical Technologies in the Biomedical and Life Sciences, 2017, 1067, 45-52.	2.3	42
47	Use of metal composite MOFâ€5â€Ag ₂ Oâ€NPs as an adsorbent for the removal of Auramine O dye under ultrasound energy conditions. Applied Organometallic Chemistry, 2018, 32, e4007.	3.5	42
48	Sonochemical-solvothermal synthesis of guanine embedded copper based metal-organic framework (MOF) and its effect on oprD gene expression in clinical and standard strains of Pseudomonas aeruginosa. Ultrasonics Sonochemistry, 2018, 42, 237-243.	8.2	39
49	A Bi ₂ WO ₆ /Ag ₂ S/ZnS <i>Z</i> scheme heterojunction photocatalyst with enhanced visible-light photoactivity towards the degradation of multiple dye pollutants. RSC Advances, 2019, 9, 30100-30111.	3.6	39
50	A hybrid model of support vector regression with genetic algorithm for forecasting adsorption of malachite green onto multi-walled carbon nanotubes: central composite design optimization. Physical Chemistry Chemical Physics, 2016, 18, 13310-13321.	2.8	37
51	An easily organic–inorganic hybrid optical sensor based on dithizone impregnation on mesoporous SBAâ€15 for simultaneous detection and removal of Pb(II) ions from water samples: Responseâ€surface methodology. Applied Organometallic Chemistry, 2017, 31, e3842.	3.5	36
52	A simple approach for the sonochemical loading of Au, Ag and Pd nanoparticle on functionalized MWCNT and subsequent dispersion studies for removal of organic dyes: Artificial neural network and response surface methodology studies. Ultrasonics Sonochemistry, 2018, 42, 422-433.	8.2	36
53	Application of magnetic nanomaterials in electroanalytical methods: A review. Talanta, 2021, 225, 121974.	5.5	36
54	Highly selective MXene/V2O5/CuWO4-based ultra-sensitive room temperature ammonia sensor. Journal of Hazardous Materials, 2021, 416, 126196.	12.4	36

#	Article	IF	CITATIONS
55	Preparation and characterization of monoliths HKUST-1 MOF <i>via</i> straightforward conversion of Cu(OH) ₂ -based monoliths and its application for wastewater treatment: artificial neural network and central composite design modeling. New Journal of Chemistry, 2018, 42, 10327-10336.	2.8	35
56	Molecular Imprinted Poly(2,5-benzimidazole)-Modified VO ₂ –CuWO ₄ Homotype Heterojunction for Photoelectrochemical Dopamine Sensing. Analytical Chemistry, 2022, 94, 6781-6790.	6.5	35
57	Preparation and characterization of a novel optical chemical sensor for determination of trace amounts of Praseodymium ion by UV/Vis spectrophotometry. Sensors and Actuators B: Chemical, 2017, 242, 586-594.	7.8	34
58	Zinc oxide nanorodâ€loaded activated carbon for ultrasoundâ€assisted adsorption of safranin O: Central composite design and genetic algorithm optimization. Applied Organometallic Chemistry, 2018, 32, e4099.	3.5	32
59	Natural Source-Based Graphene as Sensitising Agents for Air Quality Monitoring. Scientific Reports, 2019, 9, 3798.	3.3	32
60	Application of central composite design for optimization of preconcentration and determination of La (III) ion in water samples using the SBA-15-HESI and SBA-15-HESI-Fe 3 O 4 -NPs sorbents. Journal of Environmental Chemical Engineering, 2017, 5, 5233-5240.	6.7	31
61	Fe/Co-chalcogenide-stabilized Fe3O4 nanoparticles supported MgAl-layered double hydroxide as a new magnetically separable sorbent for the simultaneous spectrophotometric determination of anionic dyes. Microchemical Journal, 2020, 152, 104431.	4.5	31
62	A dual surface inorganic molecularly imprinted Bi2WO6-CuO/Ag2O heterostructure with enhanced activity-selectivity towards the photocatalytic degradation of target contaminantst. Photochemical and Photobiological Sciences, 2020, 19, 943-955.	2.9	25
63	Hydrophilic magnetic molecularly imprinted resin in PVDF membrane for efficient selective removal of dye. Journal of Environmental Management, 2021, 300, 113707.	7.8	25
64	Gold anchoring to CuFe2F8(H2O)2 oxyfluoride for robust sono-photodegradation of Rhodamine-B. Journal of Cleaner Production, 2021, 313, 127916.	9.3	24
65	An asymmetric Schiff base-functionalized gold nanoparticle-based colorimetric sensor for Hg ²⁺ ion determination: experimental and DFT studies. Analytical Methods, 2021, 13, 2603-2611.	2.7	22
66	Adsorption of methyl red onto palladium nanoparticles loaded on activated carbon: experimental design optimization. Desalination and Water Treatment, 2016, 57, 22646-22654.	1.0	21
67	Efficient adsorption of erythrosine and sunset yellow onto modified palladium nanoparticles with a 2-diamine compound: Application of multivariate technique. Journal of Industrial and Engineering Chemistry, 2017, 48, 43-55.	5.8	20
68	Processing Guar Gum into polyester fabric based promising mixed matrix membrane for water treatment. Carbohydrate Polymers, 2021, 254, 116806.	10.2	19
69	Potentiometric Ion-Selective Electrode Based on a New Single Crystal Cadmium(II) Schiff Base Complex for Detection of Fluoride Ion: Central Composite Design Optimization. IEEE Sensors Journal, 2019, 19, 413-425.	4.7	18
70	Development of Cigarette Carbonaceous Hydrochar/ZIF-67-Based Fluids for CO ₂ Capture from a Gas Stream in a Packed Column: Mass-Transfer Performance Evaluation. Energy & Fuels, 2020, 34, 7295-7306.	5.1	18
71	Corn derivative mesoporous carbon microspheres supported hydrophilic polydopamine for development of new membrane: Water treatment containing bovine serum albumin. Chemosphere, 2020, 259, 127440.	8.2	18
72	S-scheme NIR-edge Ag3CuS2/VO2 heterostructure for photo-oxidation/reduction of methylene blue/Cr (VI). Applied Surface Science, 2022, 590, 153118.	6.1	18

#	Article	IF	CITATIONS
73	Preparation of chitosan functionalized endâ€capped Agâ€NPs and composited with Fe ³ O ⁴ â€NPs: Controlled release to pHâ€responsive delivery of progesterone and antibacterial activity against <i>pseudomonas aeruginosa (PAOâ€1)</i> . Applied Organometallic Chemistry, 2018, 32, e3921.	3.5	17
74	Electrostatically controlled plasmonic effects of gold nanoparticles with indigo-carmine functionation for rapid and straightforward colorimetric detection of Cu2+ ions. Spectrochimica Acta - Part A: Molecular and Biomolecular Spectroscopy, 2020, 230, 118026.	3.9	17
75	Optimization of solid phase dispersive fieldâ€assisted ultrasonication for the extraction of auramine O and crystal violet dyes using central composite design. Applied Organometallic Chemistry, 2018, 32, e4181.	3.5	16
76	Robust charge carrier by Fe3O4 in Fe3O4/WO3 core-shell photocatalyst loaded on UiO-66(Ti) for urea photo-oxidation. Chemosphere, 2021, 267, 129206.	8.2	16
77	Preparation of silver nanoparticle loaded on activated carbon and its application for removal of malachite green from aqueous solution. Synthesis and Reactivity in Inorganic, Metal Organic, and Nano Metal Chemistry, 2016, , 00-00.	0.6	15
78	Sonochemical incorporated of cytosine in Cu-H2bpdc as an antibacterial agent against standard and clinical strains of Proteus mirabilis with rsbA gene. Ultrasonics Sonochemistry, 2018, 44, 223-230.	8.2	15
79	Lead (II) adsorption from aqueous solutions onto modified ag nanoparticles: Modeling and optimization. Environmental Progress and Sustainable Energy, 2016, 35, 743-749.	2.3	14
80	Colorimetric determination of F-, Br- and I- ions by Ehrlich's bio-reagent oxidation over enzyme mimic like gold nanoparticles: Peroxidase-like activity and multivariate optimization. Spectrochimica Acta - Part A: Molecular and Biomolecular Spectroscopy, 2020, 226, 117606.	3.9	14
81	Fluid based cigarette carbonaceous hydrochar supported ZIF-8 MOF for CO2 capture process: The engineering parameters determination for the packed bed column design. Chemical Engineering and Processing: Process Intensification, 2020, 153, 108001.	3.6	13
82	Hierarchical Fe ₂ O ₃ /Na ₂ WO ₄ Nanofibers Supported on Conductive Carbon Cloth as a High-Performance Supercapacitor. Energy & Fuels, 2021, 35, 11551-11562.	5.1	13
83	Schiff Base Impregnated Plasticized Polyvinyl Chloride Optical Sensor for Selective and Efficient Detection of Copper (II) Ion: Central Composite Design. IEEE Sensors Journal, 2015, 15, 6604-6610.	4.7	11
84	Simultaneous removal of Cu ²⁺ and Cr ³⁺ ions from aqueous solution based on Complexation with Eriochrome cyanineâ€R and derivative spectrophotometric method. Applied Organometallic Chemistry, 2018, 32, e3918.	3.5	11
85	A study to assess the knowledge and practice of medical professionals on radiation protection in in interventional radiology. Indian Journal of Radiology and Imaging, 2020, 30, 64-69.	0.8	11
86	Bi/BiPO4 nanocubes supported BiOI-BiOCI nanoplate as a heterostructured blue-light-driven photocatalyst for degradation of Auramine O. Polyhedron, 2022, 212, 115539.	2.2	6
87	Electrocatalytic membrane containing CuFeO2/nanoporous carbon for organic dye removal application. Chemical Engineering Research and Design, 2022, 183, 345-356.	5.6	5
88	In vitro curcumin delivery and antibacterial activity of RuS 2 and RuO 2 nanoparticles loaded chitosan biopolymer. Applied Organometallic Chemistry, 2018, 32, e4035.	3.5	3
89	Developing a new colorimetric bioassay for iodide determination based on gold supported iridium peroxidase catalysts. New Journal of Chemistry, 2020, 44, 5588-5597.	2.8	3